Journal of Materials Chemistry A

Accepted Manuscript

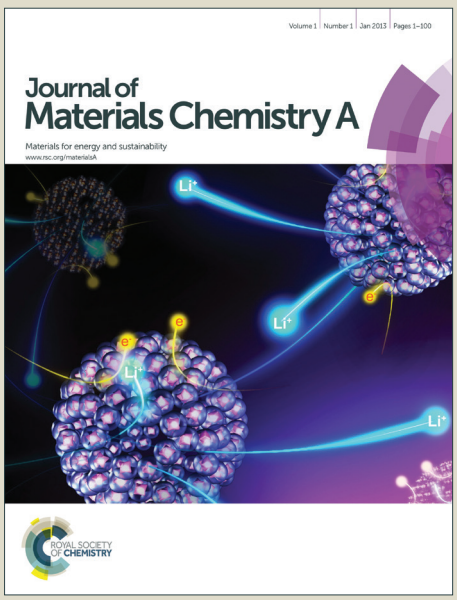

ROYAL SOCIETY OF CHEMISTRY

www.rsc.org/materialsA

Journal of Materials Chemistry A

Cite this: DOI: 10.1039/c0xx00000x

COMMUNICATION

www.rsc.org/xxxxxx

Mesoporous carbon material co-doped with nitrogen and iron (Fe-N-C): Highly performing cathode catalyst for oxygen reduction reaction in alkaline electrolyte†

Xiang-Hui Yan, and Bo-Qing Xu*

Received (in XXX, XXX) Xth XXXXXXXXX 20XX, Accepted Xth XXXXXXXXX 20XX
DOI: 10.1039/b000000x

This work uncovers an ordered mesoporous carbon material co-doped with nitrogen and iron (Fe-N-C) for ORR catalysis in alkaline electrolyte, whose ORR performance surpasses most of earlier metal-free heteroatom-containing carbon materials and is comparable to conventional Pt/C in terms of half-wave potential, limiting current density and kinetic current density. Procedure for preparing this Fe-N-C catalyst is described.

The desire for zero-Pt and cheap electrocatalyst for the cathodic oxygen reduction reaction (ORR) in fuel cells has motivated many research activities. Among various non-precious metal catalysts (NPMCs) documented in literature,[1–10] nitrogen (N)-doped carbon materials (N-C) have recently evolved into metal-free ORR catalysts though their ORR performance is still far inferior to conventional Pt-based catalysts. A co-doping with non-precious transition metal elements (like Fe, Co, etc) could improve the electrocatalytic activity of the N-C materials for ORR,[11–13] though nature of the catalytically active sites in these M-N-C catalysts remains unclear.[14,15] The M-N-C catalysts are generally prepared by pyrolyzing a mixture comprising of a nitrogen-containing organic precursor, a salt of the transition metal and a carbon-based supporting material.[16,17] Due to their large surface area, conventional carbon black and activated carbons were used as the carbon supporting materials but their rich micropores could induce problems to oxygen transport and reduce the accessibility of active sites.[18] It is known that the most desirable carbon supporting materials for fuel cell electrodes would be those having good electrical conductivity, large surface area, suitable mesoporosity and high electrochemical stability.[19] We would therefore anticipate that M-N-C materials derived from ordered high-surface-area mesoporous carbons in suitable pore sizes could be more promising catalysts for the ORR catalysis.

We report herein a highly performing mesoporous Fe-N-C catalyst for ORR in alkaline electrolyte. This Fe-N-C catalyst is a partly graphitized and ordered mesoporous Fe-N-C material featuring a pore size of *ca*. 4.9 nm and a surface area of *ca*. 236 m^2 g^{-1}, which was prepared by using hexagonally ordered mesoporous silica (SBA-15) as a hard template, $FeCl_3$ as the metal precursor, and aniline (ANI) as the only precursor source for both carbon and nitrogen, followed by SiO_2-removal and pyrolysis. It will be shown that the ORR performance of this mesoporous Fe-N-C catalyst in 0.1 M KOH surpasses most of the up-to-date metal-free carbon-based materials doped with heteroatoms such as nitrogen (N),[2,3] sulphur (S),[4,5] phosphorus (P),[6,7] iodine (I)[8] and boron (B),[9] and other M-N-C catalysts,[12,13,20,21] and is comparable to conventional Pt/C (E-TEK, 20 wt% Pt) catalyst in terms of the ORR half-wave potential and kinetic current density. Moreover, we demonstrate that this mesoporous Fe-N-C catalyst also shows remarkable stability and methanol tolerance for ORR in alkaline electrolyte. The ordered meso-porosity and Fe-doping appear to be essential to the high ORR performance when N-C and Fe-N-C samples with different porosities are compared. To our knowledge, this would be the first report on the high performance for ORR in alkaline electrolyte of PANI-derived ordered mesoporous Fe-N-C catalyst, which could shed a light on further development of high performance NPMCs for alkaline polymer electrolyte fuel cells.

The ordered mesoporous Fe-N-C catalyst was prepared according to Scheme S1†, in which the literature methodology[21] was modified by employing ANI as the precursor source for both carbon and nitrogen, and SBA-15 silica as the hard template to restrain ANI polymerization. Briefly, a self-made SBA-15 (pore diameter: *ca*. 5.6 nm, surface area: 840 m^2 g^{-1}) was immersed in aqueous HCl containing ANI, followed by stirring until ANI became adsorbed into the pores of SBA-15. Ammonium peroxydisulfate (APS) was then added to initiate polyaniline (PANI) formation, together with a simultaneous addition of a desirable quantity of $FeCl_3$; a dark green mixture was formed after 24 h of constant stirring. This dark green product was dried at 100 ^oC overnight and then subjected to carbonization by pyrolysis at 900 ^oC in flowing nitrogen (120 mL min^{-1}), followed by further treatment with NaOH solution (2M) to remove the hard template SBA-15. After extensive sequential washing with

*Innovative Catalysis Program, Key Lab of Organic Optoelectronics & Molecular Engineering, Department of Chemistry, Tsinghua University, Beijing 100084 (China), Fax: (+86)10-6279-2122, E-mail: bgxu@mail.tsinghua.edu.cn

† Electronic supplementary information (ESI) available: Experimental details, partial characterization results and experimental data.

deionized water and ethanol, the SiO_2-free sample was subjected to another hydrolysis at 900 °C. The sample obtained at termination of this second heat treatment (HT2) was denoted as PANI-xFe-HT2(SBA-15), where x refers to the Fe content (wt%). Three reference samples were also prepared using the same procedure except without using SBA-15, $FeCl_3$ and both of them, and were denoted as PANI-xFe-HT2, PANI-HT2(SBA-15) and PANI-HT2, respectively. The Fe content (x) was 4.5 wt% according to ICP-AES analysis.

Fig. 1A shows the small angle XRD diffraction patterns for the as-prepared samples and SBA-15. The three well-resolved peaks at 2θ = 0.92, 1.57, and 1.81° for SBA-15 were characteristic of the (100), (110), and (200) diffractions in an ordered 2D hexagonal mesostructure with the space group *p6mm*.[22] No diffraction in the region of 2θ = 0.6 ~ 4° for the PANI-HT2 and PANI-4.5Fe-HT2 samples, prepared in the absence of SBA-15, demonstrates that these two samples had no regular meso-porosity. In contrast, both PANI-HT2(SBA-15) and PANI-4.5Fe-HT2(SBA-15), prepared in the presence of SBA-15, show one broad peak assignable to the (100) diffraction, though the peak intensity was much lower than in the case of SBA-15 and the other two peaks at 2θ = 1.57 and 1.81° for SBA-15 were barely observed. These results reveal that the preparations using SBA-15 as the template had indeed led to carbon products with ordered meso-porosity replicating the SiO_2-wall of the template SBA-15.

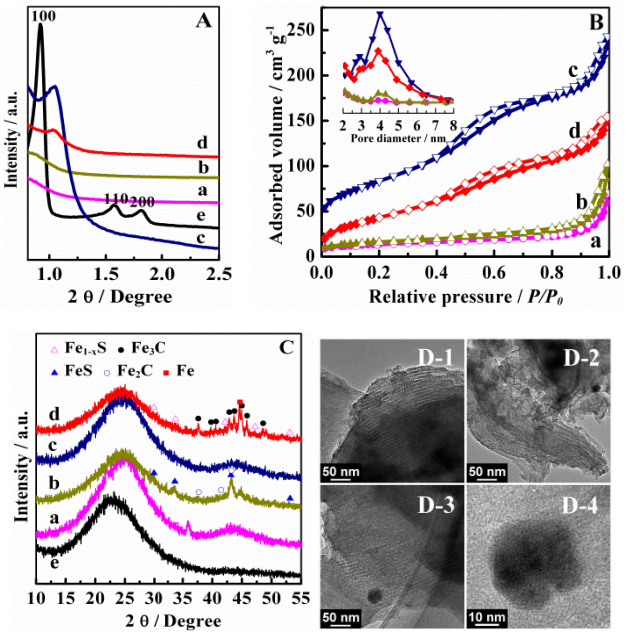

Fig. 1 (A) Small angle XRD patterns, (B) N_2 adsorption/desorption isotherms and pore size distributions (inset), and (C) wide angle XRD patterns of PANI-HT2 (a), PANI-4.5Fe-HT2 (b), PANI-HT2(SBA-15) (c), PANI-4.5Fe-HT2(SBA-15) (d), SBA-15 (e). (D) Representative TEM images of PANI-4.5Fe-HT2(SBA-15) (d).

Fig. 1B shows the nitrogen adsorption-desorption isotherms of the samples; the isotherm for SBA-15 is shown in Fig. S1†. The hysteresis loop in the high relative pressure range ($P/P_0 > 0.8$) on the isotherms for both PANI-HT2 and PANI-4.5Fe-HT2 is indicative of irregular pores constructed from aggregated particles.[27] The PANI-HT2(SBA-15) and PANI-4.5Fe-HT2(SBA-15) samples show typical type-IV isotherms; besides the hysteresis loop at the high P/P_0 range, they give also an additional H1 hysteresis loop in intermediate P/P_0 region ($0.4 < P/P_0 < 0.8$), being characteristic of mesoporous materials.[22] The richness in meso-porosity of these two samples are well demonstrated by the pore size distribution (PSD) curves, shown as an inset of Fig. 1B; the pore sizes are mainly in the range of 3.0 ~ 5.5 nm. In contrast, the PSD curves for the other two samples (PANI-HT2 and PANI-4.5Fe-HT2) feature only very limited meso-porosity. Table S1† gives a clear comparison of the textural data for all of the four samples prepared in this work.

Fig. 1C shows the normal wide-angle XRD diffraction patterns, from which information on iron entities in the samples could be extracted. The broad peak at around 2θ = 23° for SBA-15 signifies amorphous silica and the two broad peaks at 2θ = 24.7 and 43.2° in the patterns for the four PANI-derived samples correspond to (002) and (101) diffractions of graphitic carbon, respectively.[24] The patterns for PANI-4.5Fe-HT2 and PANI-4.5Fe-HT2(SBA-15) show the signals characteristic of Fe-involving crystallites, signifying the presence of doped iron species in these two samples. The iron species doped in PANI-4.5Fe-HT2 without ordered meso-porosity involve $Fe_{1-x}S$ (JCPDS 29-0725), FeS (JCPDS 37-0477), metallic Fe (JCPDS 06-0696), Fe_2C (JCPDS 36-1249) and Fe_3C (JCPDS 35-0772) while only three of the five species (*i.e.*, $Fe_{1-x}S$, Fe and Fe_3C) are detected in PANI-4.5Fe-HT2(SBA-15) with oerdered meso-porosity. Semi-quantitatively, FeS and Fe_2C are the dominant iron species in PANI-4.5Fe-HT2 while Fe_3C and metallic Fe in the ordered mesoporous PANI-4.5Fe-HT2(SBA-15). The feature of PANI-4.5Fe-HT2(SBA-15) with an ordered meso-porosity is further confirmed by the TEM images shown in Fig. 1D, which clearly reveal large ordered domains with stripe-like and hexagonal fringes, as observed in the documented TEM images for the SBA-15.[22] In combination with an EDX probe (Fig. S2†), the iron species appeared in the TEM images as differently sized particles encapsulated by graphitic carbon layers. Besides a demonstration of the feasibility of using ordered mesoporous SBA-15 as the hard template for fabricating mesoporous structured carbons, these results also uncover that the SBA-15 template also affected the chemical states and their relative content of the doped iron species in the final samples.

XPS measurements were carried out to determine the surface composition and chemical states of nitrogen species in the PANI-derived samples. The survey spectra (Fig. S3†) feature strong and distinct signals for C, N and O in all samples but very weak signals for Fe and S in both PANI-4.5Fe-HT2 and PANI-4.5Fe-HT2(SBA-15). Quantitatively (Table S1 and S2†), the N contents in the mesoporous PANI-HT2(SBA-15) and PANI-4.5Fe-HT2(SBA-15) are 8.3 and 7.6 at.%, respectively, about twice those in their PANI-HT2 (5.0 at.%) and PANI-4.5Fe-HT2 (4.6 at.%) counterparts prepared in the absence of SBA-15. These results disclose that the mesoporous template also functioned to significantly reduce the nitrogen loss or promoted N-doping during the pyrolysis steps. Fig. 2 shows the N 1s spectra for each of the four samples. Deconvolution of these spectra led to four signals with binding energies centred at 398.4, 399.5, 401.0 and 403.3−404.8 eV, assignable to pyridinic N, pyrrolic N, quaternary N and oxidized pyridinic N, respectively.[2,3,17] These N-species and their percentages are also listed in Table S1† for clarity. Note

that the pyrrolic and oxidized pyridinic N-species are not observed only for the PANI-HT2 sample with neither ordered meso-porosity nor Fe-doping. And, the percentages of pyrrolic and oxidized pyridinic N-species in the nitrogen-rich PANI-HT2(SBA-15) are remarkably lower than in PANI-4.5Fe-HT2 and PANI-4.5Fe-HT2(SBA-15), which would manifest that the occurrence of Fe-doping could be essential in promoting the formation of the pyrrolic and oxidized pyridinic N-species. Thus, the present approach using a sacrificing SBA-15 as the template and $FeCl_3$ as the Fe-dope for preparing Fe-N-C catalysts proves to be effective for producing ordered mesoporous structures with tuneable chemical states for the doped N- and Fe-species.

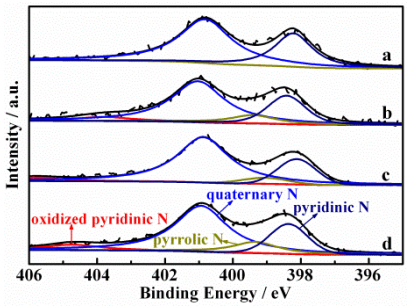

Fig. 2 XPS N 1s spectra of PANI-HT2 (a), PANI-4.5Fe-HT2 (b), PANI-HT2(SBA-15) (c) and PANI-4.5Fe-HT2(SBA-15) (d).

Table 1 Electrocatalytic properties for the cathode ORR in alkaline electrolyte (0.1 M KOH) of the PANI-derived catalysts

Sample	E_{onset} (V)	$E_{1/2}$ (V)	J_L (V)	J_k (mA cm^{-2}) 0.82 V	0.87 V
PANI-HT2	0.90	0.68	-	0.29	0.08
PANI-4.5Fe-HT2	0.91	0.75	3.74	0.74	0.15
PANI-HT2(SBA-15)	0.92	0.78	3.97	1.44	0.28
PANI-4.5Fe-HT2(SBA-15)	0.95	0.84	4.50	7.40	1.77
Pt/C (E-TEK, 20 wt% Pt)	0.99	0.83	4.60	6.30	1.60

The E_{onset} is defined as the potential at which the ORR generates a current density of −0.02 mA·cm^{-2}.[13] The potentials are given with respect to RHE.

The catalytic performance of the PANI-derived samples towards ORR was studied by linear sweep voltammetry (LSV) using a rotating disk electrode (RDE) in O_2-saturated alkaline electrolyte; unless otherwise specified the catalyst loading of 610 μg·cm^{-2}.† Note that this loading amount was previously used by Zelenay et al. in their earlier studies on Fe-N-C catalysts for ORR in acidic electrolyteon.[11,17] A conventional Pt/C (20 wt% E-TEK) catalyst was also measured for reference by applying a catalyst loading of 102 μg·cm^{-2} or 20 μg_{Pt}·cm^{-2}.[11,21,25] Fig. 3A shows the polarization curves, from which the onset potential (E_{onset}), half-wave potential ($E_{1/2}$) and limiting current density (J_L) are extracted and listed in Table 1. PANI-HT2 with neither ordered meso-porosity nor Fe-doping produced the lowest E_{onset} and $E_{1/2}$, and a plateau due to diffusing limitation for measuring J_L could not be reached, suggesting a poor ORR performance with an overall kinetic-controlled process in the measured potential range (0~1.0 V). A little higher E_{onset} and $E_{1/2}$, together with a measurable J_L (3.74 mA cm^{-2}), were obtained on PANI-4.5Fe-HT2 with doped Fe but without ordered meso-porosity. Still higher E_{onset}, $E_{1/2}$ and J_L were registered on PANI-HT2(SBA-15) free of Fe but with a rich ordered meso-porosity, see the inset of Fig. 1B. Notably, the Fe-doped mesoporous PANI-4.5Fe-HT2(SBA-15) showed the most prominent ORR performance, whose polarization curve almost overlapped with that for Pt/C. Specifically, the E_{onset} (0.95 V) was only 40 mV lower but $E_{1/2}$ (0.84 V) even 10 mV higher on this PANI-4.5Fe-HT2(SBA-15) than on Pt/C. The J_L data on PANI-4.5Fe-HT2(SBA-15) (4.50 mA·cm^{-2}) and Pt/C (4.60 mA·cm^{-2}) appeared also comparable. These results signify that the ordered mesoporous structured carbons co-doped with N and Fe would be responsible for the high ORR activity of PANI-4.5Fe-HT2(SBA-15). In the high potential range (0.62~0.89 V), this PANI-4.5Fe-HT2(SBA-15) catalyst always produced some higher current density or faster ORR kinetics than did Pt/C (Fig. 3A).

The rotation speed (ω) was changed between 600 and 2200 rpm to further investigate the ORR kinetics. Fig. 3B presents as representatives the LSVs for PANI-4.5Fe-HT2(SBA-15), which are similar to those documented in literature for Pt/C and efficient NPMCs.[15,26] The overlapped J data at potentials higher than $E_{1/2}$ (0.84 V) or on the side of low over-potentials feature an intrinsic kinetics while the increase in J with ω at potentials lower than $E_{1/2}$ or on the side of high over-potentials an diffusion-disturbed kinetics. The plateau at further lower potentials measures J_L at each specific ω. The inset of Fig. 3B shows the corresponding Koutecky-Levich (K-L) plots (J vs. $\omega^{-1/2}$) at various electrode potentials. The good linearity of these K-L plots and their similar slopes in the potential range of 0.37~0.77 V would demonstrate a first-order ORR kinetics at these potentials.[9] The slopes of these plots were then used to quantitatively measure the number of transferred electrons (n) per O_2-reduction,[27] which are found to be comparable with those on Pt/C (Fig. S4†). The numbers registered on PANI-HT2 (n = 2.5~2.9) reveal that a 2-electron pathway dominated the ORR process, in agreement with many earlier reports on N-C catalysts.[13,28,29] However, the significantly higher numbers registered on PANI-HT2(SBA-15) (n = 3.0~4.0) would imply that the rich meso-porosity in the PANI-derived N-C materials could somehow "steer" ORR in favour of the 4-electron pathway, which is most desirable on consideration of energy efficiency. The still higher numbers on PANI-4.5Fe-HT2 and PANI-4.5Fe-HT2(SBA-15) (n = 3.4~4.0) would further suggest that Fe-doping is more critical to the selectivity of ORR towards the 4-electron pathway. This high selectivity of the present Fe-N-C catalysts is in line with earlier reports on other NPMCs.[2,12,25,26,30]

The kinetic current density (J_k), which measures the current in absence of any mass transfer effect, is an important parameter in evaluating the intrinsic activity of a catalyst. To ensure reliability and accuracy, the well-known equation: $1/J_k = 1/J - 1/J_L$ was applied to measure the J_k data at 0.82 and 0.87 V because at these potentials the requirement for $J < J_L/2$[31,32] can be strictly satisfied (Fig. 3A). The resultant J_k data are also listed in Table 1, which give an activity rank of PANI-HT2 < PANI-4.5Fe-HT2 < PANI-HT2(SBA-15) < PANI-4.5Fe-HT2(SBA-15). This rank is consistent with the activity order according to the E_{onset} and $E_{1/2}$ data, shown also in the same table. Specifically, the data of J_k at 0.87 V for PANI-4.5Fe-HT2 (0.15 mA·cm^{-2}), PANI-HT2(SBA-15) (0.28 mA·cm^{-2}) and PANI-4.5Fe-HT2(SBA-15) (1.77 mA·cm^{-2}) are about 2, 4 and 20 times that for PANI-HT2 (0.08 mA·cm^{-2}), respectively. It should be noted that the difference in

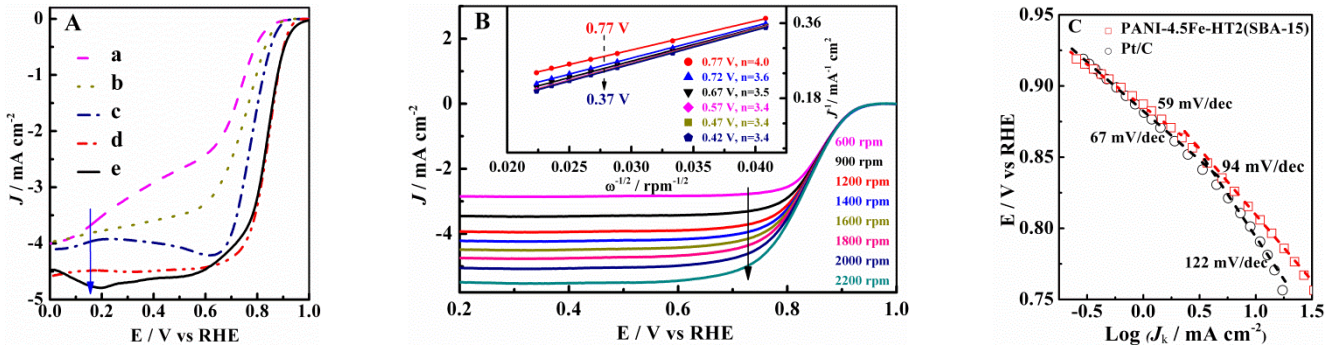

Fig. 3 (A) Polarization curves of PANI-HT2 (a), PANI-4.5Fe-HT2 (b), PANI-HT2(SBA-15) (c), PANI-4.5Fe-HT2(SBA-15) (d) and Pt/C (e) in O_2-saturated 0.1 M KOH at a scan rate of 10 mV s^{-1} and a rotation speed of 1600 rpm. (B) Polarization curves of PANI-4.5Fe-HT2(SBA-15) at various rotation speeds, and their derived Koutecky-Levich plots (J^{-1} vs. $\omega^{-1/2}$) at different potentials (inset). (C) Tafel plots for PANI-4.5Fe-HT2(SBA-15) and Pt/C catalysts.

activity between PANI-4.5Fe-HT2 and PANI-4.5Fe-HT2(SBA-15) is significantly higher than those between PANI-HT2 and PANI-4.5Fe-HT2, PANI-HT2 and PANI-HT2(SBA-15), as well as PANI-HT2(SBA-15) and PANI-4.5Fe-HT2(SBA-15). These data demonstrate again that both the meso-porosity and Fe-doping were essential to the excellent ORR performance of PANI-4.5Fe-HT2(SBA-15). Noticeably, the J_k data for this PANI-4.5Fe-HT2(SBA-15) (7.40 mA cm^{-2} at 0.82 V and 1.77 mA cm^{-2} at 0.87 V) are even higher than those for Pt/C (6.30 mA cm^{-2} at 0.82 V and 1.60 mA cm^{-2} at 0.87 V).

The superior ORR performance of the present PANI-4.5Fe-HT2(SBA-15) to conventional Pt/C is also supported by the Tafel plots shown in Fig. 3C. In the potential region of slow ORR kinetics involving no or little diffusion effect (*i.e.*, 0.85 < E < 0.92 V), the two catalysts produced very similar Tafel slopes, 59 mV/dec for PANI-4.5Fe-HT2(SBA-15) and 67 mV/dec for Pt/C, revealing similar kinetic features or mechanisms on both catalysts. In the potential region of fast ORR kinetics involving significant diffusion effect (*i.e.*, 0.75 < E < 0.85 V), however, the Tafel slope for PANI-4.5Fe-HT2(SBA-15) (94 mV/dec) was significantly smaller than that for Pt/C (122 mV/dec). These data indicate that the present PANI-4.5Fe-HT2(SBA-15) could be more advantageous to conventional Pt/C catalyst for producing faster ORR kinetics.

The above activity comparison between the ordered mesoporous PANI-4.5Fe-HT2(SBA-15) and Pt/C ignored the difference in catalyst loading (PANI-4.5Fe-HT2(SBA-15): 610 μg·cm^{-2}, Pt/C: 102 μg·cm^{-2}), though a much higher loading for NPMC could be acceptable in practice because the price of Pt/C could be two orders of magnitude higher. We show in Fig. S5† the effect of catalyst loading on the ORR activity of PANI-4.5Fe-HT2(SBA-15) by varying the loading between 102 and 610 μg·cm^{-2}. Table S3† compares the J_k, E_{onset} and $E_{1/2}$ data for ORR of this PANI-4.5Fe-HT2(SBA-15) with those for NPMCs in literature.[2–9,21,26,33–37] As long as the comparison is made at similar catalyst loadings, this ordered mesoporous PANI-4.5Fe-HT2(SBA-15) always appeared as the most active NPMC except a metal-free sulfur-nitrogen co-doped carbon foams with hierarchical pore structures (SN-CF) reported in ref 40. Even at the same loadings (e.g., 102 μg·cm^{-2}), the activity by J_k of this mesoporous PANI-4.5Fe-HT2(SBA-15) was also remarkable, reaching a half of that of Pt/C (Table S3†).

Therefore, the ordered meso-porosity and Fe-doping are the two keys to the remarkable high ORR activity of PANI-4.5Fe-HT2(SBA-15). Although there are earlier documents on the importance of an ordered meso-porosity and Fe-doping for improving the ORR performance in NPMCs,[29,38–40] this present work provides a new one-pot approach by using ANI as sole source for both carbon and nitrogen and SBA-15 for generating "*ordered meso-porosity*" in Fe-N-C materials. Besides, the high activity of this PANI-4.5Fe-HT2(SBA-15) catalyst would also have relation with its large surface area (236 m^2 g^{-1}), high nitrogen content (7.6 at.%) and relatively more uniform Fe-N-C structures, which could also be affected by function of the ordered meso-porosity. As we addressed in the preceding discussion on the XRD and XPS results, the template SBA-15 could somehow affect the doping and chemical states of Fe and N in the samples. According to earlier studies,[29,38] the doped Fe-species in N-C materials would modify the electron property of their adjacent active carbon atoms to improve their ORR activity. Also documented is a crucial role for ORR of nitrogen-iron coordinations and/or FeN_4 moieties, generated due to interaction between the doped Fe and N during the preparation.[12,38,39] The nature of key Fe-species and their relation with co-existing N-species in the present samples remain unclear though the most active PANI-4.5Fe-HT2(SBA-15) catalyst is rich in Fe_3C and metallic Fe (Fig. 1C) and has more pyrrolic and oxidized pyridinic N-species (Fig. 2 and Table S1†). Work under progress in this laboratory is being devoted to address this issue.

We show below the on service durability of PANI-4.5Fe-HT2(SBA-15) in reference to conventional Pt/C (Fig. 4), which were evaluated by means of chronoamperometric (CA) measurement at 0.57 V (Fig. 4A) and the accelerated catalyst decay test with potential cycling for 10,000 cycles between 0.6 and 1.05 V (Fig. 4B). In Fig. 4A, the activity loss for PANI-4.5Fe-HT2(SBA15) during the test period (18000 s) was less than 2% whereas that for Pt/C was 24%. In Fig. 4B, the polarization curves for PANI-4.5Fe-HT2(SBA-15) before and after the potential cycling (10,000 cycles) were less different than were the curves for Pt/C. These results would indicate that the long-term durability of the PANI-4.5Fe-HT2(SBA-15) would be at least no worse, if not significantly better, than that of Pt/C catalyst. As it would be anticipated, PANI-4.5Fe-HT2(SBA-15) would also show an outstanding resistance against methanol

oxidation, which was confirmed with the data shown in Fig.S6†. In combination with its high activity and good service durability, this excellent methanol tolerance capability would make PANI-4.5Fe-HT2(SBA-15) of particular promising for advanced cathode ORR catalysis in alkaline methanol fuel cells.

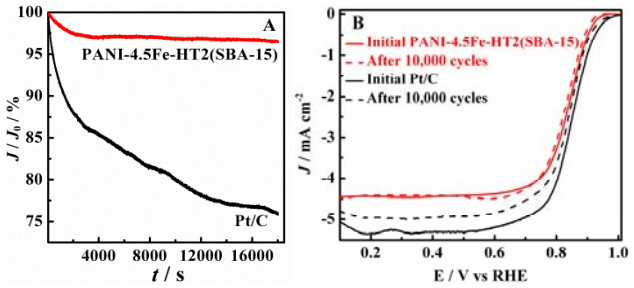

Fig. 4 Chronoamperometric (A) and accelerated catalyst-decay evaluations (B) of PANI-4.5Fe-HT2(SBA-15) and Pt/C catalysts. The RDE rotation speed was 900 rpm in (A) and 1600 rpm in (B). The solid and dashed curves in (B) refer, respectively, to the polarization before and after the potential cycling for 10000 cycles between 0.6 and 1.05 V.

In summary, the present report discloses an unprecedented approach for ordered mesoporous carbon materials co-doped with nitrogen and iron (Fe-N-C), which is characterized by using an ordered mesoporous SiO_2 (SBA-15) as the hard template for ANI polymerization in presence of $FeCl_3$ and ANI as the sole precursor source for both carbon and nitrogen. The resultant Fe-N-C material showed high catalytic activity for the cathode ORR in alkaline electrolyte, whose ORR performance surpasses most of earlier metal-free carbon materials doped with heteroatoms (such as N, S, P, I and B) and other M-N-C catalysts in literature and is comparable, if not superior, to conventional Pt/C in terms of half-wave potential, limiting current density and kinetic current density. This ordered mesoporous Fe-N-C catalyst also showed higher service stability than conventional Pt/C and would offer remarkable methanol tolerance capability during ORR. This novel approach for mesoporous Fe-N-C materials could have flexibilities in tailoring the composition, meso-porosity, chemical states of the doped N- and Fe-species, which may open a space for designed preparation of M-N-C and other NPMCs with further higher ORR performance.

Acknowledgements

This work was supported by the National Basic Research Program of China (2013CB933103) and NSF (grant: 21221062) of China.

References

1 a). A. Morozan, B. Jousselme and S. Palacin, *Energy Environ. Sci*., 2011, **4**, 1238; b). H. Jin, H. M. Zhang, H. X. Zhong, and J. L. Zhang, *Energy Environ. Sci*., 2011, **4**, 3389; c). Y. Zheng, Y. Jiao, J. Chen, J. Liu, J. Liang, A. J. Du, W. M. Zhang, Z. H. Zhu, S. C. Smith, M. Jaroniec, G. Q. Lu and S. Z. Qiao, *J. Am. Chem. Soc*., 2011, **133**, 20116.
2 S. B. Yang, X. L. Feng, X. C. Wang and K. Müllen, *Angew. Chem. Int. Ed*., 2011, **50**, 5339.
3 S. Shanmugam and T. Osaka, *Chem. Comm*., 2011, **47**, 4463.
4 Z. Yang, Z. Yao, G. F. Li, G. Y. Fang, H. G. Nie, Z. Liu, X. M. Zhou, X. A. Chen and S. M. Huang, *ACS Nano*, 2012, **6**, 205.
5 J. Sa, C. Park, H. Y. Jeong, S.-H. Park, Z. Lee, K. T. Kim, G.-G. Park and S. H. Joo, *Angew. Chem. Int. Ed*., 2014, **53**, 1.
6 Z. W. Liu, F. Peng, H. J. Wang, H. Yu, W. X. Zheng and J. Yang, *Angew. Chem. Int. Ed*., 2011, **50**, 3257.
7 D. S. Yang, D. Bhattacharjya, S. Inamdar, J. Park and J. S. Yu, *J. Am. Chem. Soc*., 2012, **134**, 16127.
8 Z. Yao, H. G. Nie, Z. Yang, X. M. Zhou, Z. Liu and S. M. Huang, *Chem. Comm*., 2012, **48**, 1027.
9 Z. H. Sheng, H. L. Gao, W. J. Bao, F. B. Wang and X. H. Xia, *J. Mater. Chem*., 2012, **22**, 390.
10 a). Y. J. Zhang, K. Fugane, T. Mori, L. Niu and J. H. Ye, *J. Mater. Chem.,* 2012, **22**, 6575; b). Z. Schnepp, Y. J. Zhang, M. J. Hollamby, B. R. Pauw, M. Tanaka, Y. Matsushitad and Y. Sakka, *J. Mater. Chem. A*, 2013, **1**, 13576; c). S. Yasuda, L. Yu, J. Kima and K. Murakoshi, *Chem. Comm*., 2011, **49**, 9627.
11 G. Wu, K. L. More, C. M. Johnston and P. Zelenay, *Science*, 2011, **332**, 443.
12 K. Parvez, S. B Yang, Y. Hernandez, A. Winter, A. Turchanin, X. L. Feng and K. Müllen, *ACS Nano*, 2012, **6**, 9841.
13 X. H. Yan, G. R. Zhang and B. Q. Xu, *Chin. J. Catal*. **2013**, *34*, 1992.
14 P. H. Matter and U. S. Ozkan, *Catal. Lett*. 2006, **109**, 115.
15 M. S. Thorum, J. M. Hankett and A. A. Gewirth, *J. Phys. Chem. Lett*., 2011, **2**, 295.
16 M. Lefèvre, E. Proietti, F. Jaouen and J. P. Dodelet, *Science*, 2009, **324**, 71.
17 G. Wu, C. M. Johnston and P. Zelenay, *J. Mater. Chem*., 2011, **21**, 11392.
18 S. Sharma and B. G. Pollet, *J. Power Sources*, 2012, **208**, 96.
19 A. L. Dicks, *J. Power Sources*, **2006**, *156*, 128.
20 Q. Liu and J. Y. Zhang, *Langmuir*, 2013, **29**, 3821.
21 R. Silva, D. A. Voiry, M. Chhowalla and T. Asefa, *J. Am. Chem. Soc*., 2013, **135**, 7823.
22 D. Y. Zhao, Q. S. Huo, J. L. Feng, B. F. Chmelka and G. D. Stucky, *J. Am. Chem. Soc*., 1998, **120**, 6024.
23 S. Y. Chen and S. Cheng, *Chem. Mater*., 2007, **19**, 3041.
24 Y. G. Wang, C. L. Zhang, S. F. Kang, B. Li, Y. Q. Wang, L. Q. Wang and X. Li, *J. Mater. Chem*., 2011, **21**, 14420.
25 Y. G. Li, H. L. Wang, J. G. Zhou, J. Wang, T. Regier and H. J. Dai, *Nature Mater*., 2011, **10**, 780.
26 H. X. Zhong, H. M. Zhang, Z. Xu, Y. F. Tang and J. X. Mao, *ChemSusChem*, 2012, **5**, 1698.
27 A. J. Bard and L. R. Faulkner, Electrochemical Methods: Fundamentals and Applications, John Wiley & Sons, New York, 2nd edn., 2001, ch. 9, pp. 339-343.
28 Y. M. Tan , C. F. Xu , G. X. Chen, X. L. Fang, N. F. Zheng and Q. J. Xie, *Adv. Funct. Mater*., 2012, **22**, 4584.
29 G. Liu, X. G. Li, P. Ganesan and B. N. Popov, *Appl. Catal. B*, 2009, **93**, 156.
30 K. P. Gong, F. Du , Z. H. Xia, M. Durstock and L. M. Dai, *Science* 2009, **323**, 760.
31 K. J. J. Mayrhofer, D. Strmcnik, B. B. Blizanac, V. Stamenkovic, M. Arenz and N. M. Markovic, *Electrochim. Acta*, 2008, **53**, 3181.
32 K. Ke, K. Hiroshima, Y. Kamitaka, T. Hatanaka and Y. Morimoto, *Electrochim. Acta*, 2012, **72**, 120.
33 J. Liang, Y. Zheng, J. Chen, J. Liu, D. Hulicova-Jurcakova, M. Jaroniec and S. Z. Qiao, *Angew. Chem. Int. Ed*., 2012, **51**, 1.
34 Y. G. Li, W. Zhou, H. L. Wang1, L. M. Xie, Y. Y. Liang, F. Wei, J. C. Idrobo, S. J. Pennycook and H. J. Dai, *Nature Nanotech*., 2012, **7**, 394.
35 Q. Cui, L. S. J. Chao, P. H. Wang, Z. Y. Bai, H. Yan, K. Wang and L. Yang, *RSC Adv.*, DOI: 10.1039/C3RA44958K
36 Z. Liu, H. G. Nie, Z. Yang, J. Zhang, Z. P. Jin, Y. Q. Lu, Z. B. Xiao and S. M. Huang, *Nanoscale,* 2013, **5**, 3283.
37 H. L. Jiang, Y. H. Su, Y. H. Zhu, J. H. Shen, X. L. Yang, Q. Feng and C. Z. Li, *J. Mater. Chem. A*, 2013, **1**, 12074.
38 D. H. Deng, L. Yu, X. Q. Chen, G. X. Wang, L. Jin, X. L. Pan, J. Deng, G. Q. Sun and X. H. Bao, *Angew. Chem. Int. Ed*., 2013, **52**, 371.
39 Z. X. Wu, Y. Y. Lv, Y. Y. Xia, P. A. Webley and D. Y. Zhao, *J. Am. Chem. Soc*., 2011, **133**, 206.
40 a). K. Kwon, Y. J. Sa, J. Y. Cheon and S. H. Joo, *Langmuir*, 2012, **134**, 2236; b). M. Lefèvre, J. P. Dodelet and P. Bertrand, *J. Phys. Chem. B*, 2002, **106**, 8705; c). H. R. Byon, J. Suntivich and Y. Shao-Horn, *Chem. Mater*., 2011, **23**, 3421.

Manuscript ID TA-COM-12-2013-015300 for publication in *J. Mater. Chem. A*

Mesoporous carbon material co-doped with nitrogen and iron (Fe-N-C): Highly performing cathode catalyst for oxygen reduction reaction in alkaline electrolyte

Xiang-Hui Yan, and Bo-Qing Xu*

Table of contents entry:

An unprecedented ordered mesoporous carbon material co-doped with nitrogen and iron shows high activity for ORR catalysis in alkaline electrolyte.